n-Type Molybdenum Diselenide-Based Photoelectrochemical Cells: Evidence for Fermi Level Pinning and Comparison of the Efficiency for Conversion of Light to Electricity with Various Solvent/Halogen/Halide Combinations

Lynn F. Schneemeyer and Mark S. Wrighton*

Contribution from the Department of Chemistry, Massachusetts Institute of Technology, Cambridge, Massachusetts 02139. *Received April 21, 1980*

Abstract: Interfacial energetics for n-type $MoSe_2$ (E_g = 1.4 eV, direct) and photoelectrochemical conversion of light to electrical energy in the presence of X_n^-/X^- (X = Cl, Br, I) have been characterized in CH_3CN electrolyte solution. Data for $MoSe_2$ in $H_2O/I_3^-/I^-$ are included for comparison, along with a comparison of $MoSe_2$-based cells with MoS_2- (E_g = 1.7 eV, direct) based cells. Cyclic voltammetry for a set of reversible (at Pt electrodes) redox couples whose formal potential, $E°$, spans a range −0.8 to +1.5 V vs. SCE has been employed to establish the interface energetics of $MoSe_2$. For the redox couples having $E°$ more negative than ~−0.1 V vs. SCE, we find reversible electrochemistry in the dark at n-type $MoSe_2$. When $E°$ is somewhat positive of −0.1 V vs. SCE, we find that oxidation of the reduced form of the redox couple can be effected in an uphill sense by irradiation of the n-type $MoSe_2$ with $\geq E_g$ light; the anodic current peak is at a more negative potential than at Pt for such situations. The extent to which the photoanodic current peak is more negative than at Pt is a measure of the output photovoltage for a given couple. For $E°$ more positive than ~+0.7 V vs. SCE it would appear that this output photovoltage is constant at ~0.4 V. For a redox couple such as biferrocene ($E°(BF^+/BF)$ = +0.3 V vs. SCE) we find a photoanodic current onset at ~−0.2 V vs. SCE; a redox couple with $E°$ = 1.5 V vs. SCE shows an output photovoltage of 0.43 V under the same conditions. The ability to observe (i) photoeffects for redox reagents spanning a range of $E°$'s that is greater than the direct E_g and (ii) constant photovoltage for a range of $E°$'s evidences an important role for surface states or carrier inversion such that a constant amount of band bending (constant barrier height) is found for a couple having $E°$ more positive than ~+0.7 V vs. SCE. Conversion of $\geq E_g$ light to electricity can be sustained in CH_3CN solutions of X_n^-/X^- (X = Cl, Br, I) with an efficiency that is ordered Cl > Br > I where n-type $MoSe_2$ is used as a stable photoanode. In aqueous solution n-type $MoSe_2$ is not a stable anode in the presence of similar concentrations of Br_2/Br^- or Cl_2/Cl^-, showing an important role for solvent in thermodynamics for electrode decomposition. In CH_3CN, efficiency for conversion of 632.8-nm light to electricity has been found to be up to 7.5% for Cl_2/Cl^-, 1.4% for Br_2/Br^-, and 0.14% for I_3^-/I^-. Differences among these redox systems are output voltage and short-circuit current, accounting for the changes in efficiency. In H_2O, I_3^-/I^- yields a stable n-type $MoSe_2$-based photoelectrochemical cell with an efficiency for 632.8-nm light a little lower than that for the $CH_3CN/Cl_2/Cl^-$ solvent/redox couple system. Data for MoS_2-based cells in the $CH_3CN/X_n^-/X^-$ solvent/redox couple systems show that the efficiency again depends on X: Cl > Br > I. In $H_2O/I_3^-/I^-$ an efficiency a little lower than that for the $CH_3CN/Cl_2/Cl^-$ is obtained. $MoSe_2$-based cells are somewhat more efficient than MoS_2-based cells, but significant variations in efficiency are found depending on the electrode sample used.

Metal dichalcogenide (MY_2) semiconductor photoelectrode materials have attracted wide interest as relatively stable photoanodes.[1-3] While n-type MY_2 materials do have some favorable photoanode properties, no n-type MY_2 photoanode has been shown to be a durable electrode for O_2 evolution from H_2O. However, we have recently reported that both n-type MoS_2[4] and $MoSe_2$[5] having a direct band gap, E_g, of 1.7 and 1.4 eV, respectively, can be used as a stable photoanode for the oxidation of Cl^- in CH_3CN solution. The formal potential $E°$ of the Cl_2/Cl^- couple in CH_3CN is +1.1 V vs. SCE. The ability to effect Cl^- oxidation in CH_3CN is interesting, in part, because the $E°$ is so positive and because the Cl_2/Cl^- couple is optically transparent over most of the visible spectrum. Even for strongly acidic aqueous solutions, Cl_2 is a more powerful oxidant than O_2, and we are therefore interested in determining factors that allow Cl_2 to be generated without destruction of the MoS_2 or $MoSe_2$ photoanode surfaces.

In this article we report the results of a study of the interface energetics for n-type $MoSe_2$ in CH_3CN electrolyte solution. We have previously reported the results from a similar study of MoS_2.[4] Additionally, we report a comparison of the efficiency for conversion of light to electricity employing halogen/halide, X_n^-/X^- (X = Cl, Br, I) redox systems in cells employing an n-type $MoSe_2$ or MoS_2 photoanode. The study of interface energetics of $MoSe_2$ reveals that photoeffects can be found for redox couples having $E°$'s that span a range that is greater than the separation of the valence, E_{VB}, and conduction band, E_{CB}, edges of $MoSe_2$. Further, for $E°$'s more positive than ~+0.7 V vs. SCE, we find a photovoltage of ~0.4 V, independent of $E°$. These findings evidence a departure from the ideal model where (i) photoeffects are only possible for redox couples having $E°$ between E_{CB} and E_{VB} that are assumed to be fixed for a given electrolyte solution and (ii) maximum output photovoltage, E_B, varies with the electrochemical potential of the solution, E_{redox}, according to eq 1, where E_{FB}

$$E_B = |E_{redox} - E_{FB}| \quad (1)$$

represents the so-called flat-band potential of the semiconductor.[6,7]

(1) (a) Tributsch, H.; Bennett, J. C. *A. J. Electroanal. Chem.* **1977** *81*, 97. (b) Tributsch, H. *Z. Naturforsch, A* **1977**, *32A*, 972; *J. Electrochem. Soc.* **1978**, *125*, 1086; *Ber. Bunsenges. Phys. Chem.* **1977**, *81*, 361; **1978**, *82*, 169. (c) Gobrecht, J.; Tributsch, H.; Gerischer, H. *J. Electrochem. Soc.* **1978**, *125*, 2085. (d) Ahmed, S. M.; Gerischer, H. *Electrochim. Acta* **1979**, *24*, 705. (e) Kautek, W.; Gerischer, H.; Tributsch, H. *Ber. Bunsenges. Phys. Chem.* **1979**, *83*, 1000. (f) Tributsch, H.; Gerischer, H.; Clemen, C.; Bucher, E. *Ibid.*, **1979**, *83*, 655.

(2) (a) Lewerenz, H. J.; Heller, A.; DiSalvo, F. J. *J. Am. Chem. Soc.* **1980**, *102*, 1877. (b) Menezes, S.; DiSalvo, F. J.; Miller, B. *J. Electrochem. Soc.* **1980**, *127*, 1751.

(3) (a) Fan, F.-R. F.; White, H. S.; Wheeler, B.; Bard, A. J. *J. Electrochem. Soc.* **1980**, *127*, 518. (b) Fan, F.-R. F.; White, H. S.; Wheeler, B. L.; Bard, A. J. *J. Am. Chem. Soc.* **1980**, *102*, 5142.

(4) Schneemeyer, L. F.; Wrighton, M. S. *J. Am. Chem. Soc.* **1979**, *101*, 6496.

(5) Schneemeyer, L. F.; Wrighton, M. S.; Stacy, A.; Sienko, M. J. *Appl. Phys. Lett.* **1980**, *36*, 701.

(6) Gerischer, H. *J. Electronanal. Chem.* **1975**, *58*, 263.

(7) Bard, A. J.; Bocarsly, A. B.; Fan, F.-R. F.; Walton, E. G.; Wrighton, M. S. *J. Am. Chem. Soc.* **1980**, *102*, 3671.

0002-7863/80/1502-6964$01.00/0

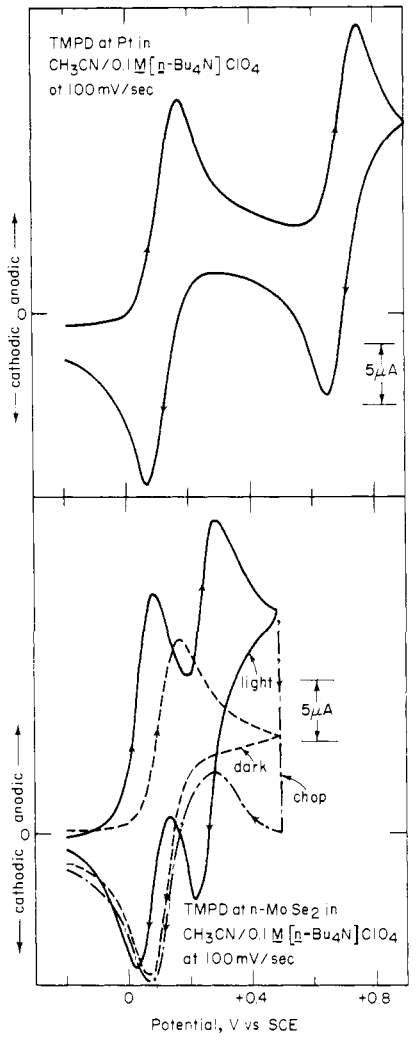

Figure 1. Comparison of cyclic voltammetry for TMPD at Pt and $MoSe_2$ (dark and illuminated and illumination discontinued at the anodic limit). Illumination was with 632.8-nm light at ~50 mW/cm².

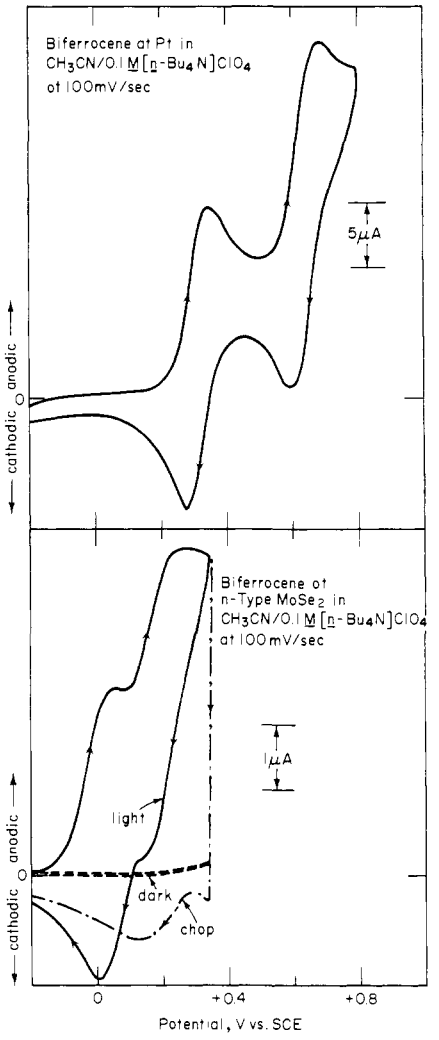

Figure 2. Comparison of cyclic voltammetry for biferrocene at Pt and at $MoSe_2$ (dark and illuminated and illumination discontinued at the anodic limit). Illumination was with 632.8-nm light at ~50 mW/cm².

It would appear that for E_{redox} more positive than +0.7 V vs. SCE in CH_3CN that the photovoltage is independent of E_{redox}. Photovoltage independent of E_{redox} reflects the fact that Fermi level pinning occurs, as has been concluded[7-9] for other small band gap photoelectrode materials such as GaAs[7,8] and Si.[7,9] Fermi level pinning can be attributed to surface states situated between E_{CB} and E_{VB}, and such states have previously been invoked for MY_2 electrodes in aqueous media.[1f] Alternatively, the E_{redox} independent photovoltage can be attributed to carrier inversion at the surface of the semiconductor when the band bending becomes large compared to the band gap of the semiconductor.[10]

Results and Discussion

a. Cyclic Voltammetry for Redox Couples at n-Type $MoSe_2$. Cyclic voltammetry of various redox couples has been compared at dark and illuminated (632.8 nm) n-type $MoSe_2$ and Pt electrodes. The measurements were made in CH_3CN/0.1 M [n-Bu_4N]ClO_4 at 25 °C under Ar. Where 632.8-nm illumination was used the light intensity was ~50 mW/cm² and was found to be sufficiently high that diffusion limited photoanodic currents were observed at the concentration of redox reagent used. The redox reagents used all exhibit reversible electrochemistry at Pt and span a range of $E°$'s from −0.8 to +1.5 V vs. SCE. All couples are fast, one-electron, outer-sphere systems where kinetics for heterogeneous electron transfer are not expected to differ significantly. Thus, differences in behavior can be attributed to differences in $E°$. Representative data from several different

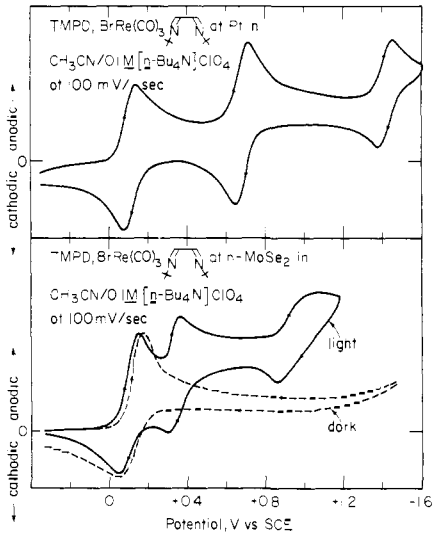

Figure 3. Comparison of cyclic voltammetry for TMPD and *fac*-BrRe(CO)$_3$L at Pt and at $MoSe_2$ (dark and illuminated). Illumination was with 632.8-nm light at ~50 mW/cm².

(8) Fan, F.-R. F.; Bard, A. J. *J. Am. Chem. Soc.* **1980**, *102*, 3677.
(9) Bocarsly, A. B.; Bookbinder, D. B.; Dominey, R. N.; Lewis, N. S.; Wrighton, M. S. *J. Am. Chem. Soc.* **1980**, *102*, 3683.
(10) (a) Gobrecht, J.; Gerischer, H.; Tributsch, H. *Ber. Bunsenges, Phys. Chem.* **1978**, *82*, 1331. (b) Kautek, W.; Gerischer, H. *Ibid.* **1980**, *84*, 645 and private communication. (c) Turner, J. A.; Manassen, J.; Nozik, A. J. *Appl. Phys. Lett.*, in press and private communication.

Table I. Comparison of Anodic Peak Current Positions for Various Redox Couples at Pt and n-Type $MoSe_2$[a]

redox couple	electrode	V vs. SCE E°[b]	$E_{PA}(A^+/A)$	$E_{PA}(A^{2+}/A^+)$
$[PQ]^{2+/+/0}$	Pt	−0.85, −0.45	−0.80	−0.40
	$MoSe_2$ (dark)		−0.80	−0.40
	$MoSe_2$ (light)		−0.80	−0.40
[decamethylferrocene]$^{+/0}$	Pt	−0.12	−0.06	
	$MoSe_2$ (dark)		−0.06	
	$MoSe_2$ (light)		−0.05	
$[TMPD]^{2+/+/0}$	Pt	0.10, 0.68	0.15	0.73
	$MoSe_2$ (dark)		0.15	
	$MoSe_2$ (light)		0.12	0.35
[biferrocene]$^{2+/+/0}$	Pt	0.30, 0.67	0.33	0.68
	$MoSe_2$ (dark)			
	$MoSe_2$ (light)		0.05	0.24
[ferrocene]$^{+/0}$	Pt	0.38	0.43	
	$MoSe_2$ (dark)			
	$MoSe_2$ (light)		0.17	
[acetylferrocene]$^{+/0}$	Pt	0.63	0.66	
	$MoSe_2$ (dark)			
	$MoSe_2$ (light)		0.36	
[1,1′-diacetylferrocene]$^{+/0}$	Pt	0.83	0.89	
	$MoSe_2$ (dark)			
	$MoSe_2$ (light)		0.50	
$[Ru(2,2'\text{-bipyridine})_3]^{3+/2+}$	Pt	1.25	1.30	
	$MoSe_2$ (dark)			
	$MoSe_2$ (light)		0.92	
fac-[$BrRe(CO)_3L$], L = glyoxalbis(*tert*-butylimine)	Pt	1.45	1.48	
	$MoSe_2$ (dark)			
	$MoSe_2$ (light)		1.05	

[a] All data are for CH_3CN/0.1 M [n-Bu_4N]ClO_4 solutions at 25 °C at a scan rate of 100 mV/s. Pt and $MoSe_2$ data for a given reductant were recorded in the same solution. Reductants are at ~1 mM concentration in each case. E_{PA} is the position of the anodic current peak. TMPD is *N*, *N*, *N*′, *N*′-tetramethyl-*p*-phenylenediamine; PQ is *N*, *N*′-dimethyl-4,4′-bipyridinium. Illumination of n-type $MoSe_2$ was with 632.8-nm light from a He–Ne laser (~50 mW/cm²). [b] These E°'s are from cyclic voltammetry at Pt-wire electrodes in the electrolyte solution used for all other studies.

$MoSe_2$ samples are given. There is some variation from sample to sample, but the essential properties are constant.

Table I summarizes data for cyclic voltammetry at a scan rate of 100 mV/s, and Figures 1–3 show cyclic voltammetry scans for several key redox couples. The redox couples can be divided into five classes depending on E°. The first class of couples are those that are reversible in the dark at n-type $MoSe_2$: these couples have E° more negative than ~−0.1 V vs. SCE including [decamethylferrocene]$^{+/0}$, E° = −0.12, and [*N*,*N*′-dimethyl-4,4′-bipyridinium]$^{2+/+/0}$, E° = −0.45 and −0.85. These couples behave essentially the same at Pt and n-type $MoSe_2$, and $\geq E_g$ illumination of the $MoSe_2$ has little, if any, effect on the cyclic voltammetric waves.

The second class of redox couples is typified by the *N*,*N*,*N*′,*N*′-tetramethyl-*p*-phenylenediamine, TMPD, system $[TMPD]^{+/0}$, E° = +0.10. For the $[TMPD]^{+/0}$ system (Figure 1), we find that the $[TMPD]^0 \rightarrow [TMPD]^+$ oxidation at n-type $MoSe_2$ can be effected in the dark, but illumination of the $MoSe_2$ with $\geq E_g$ light results in a negative shift of both the anodic current onset and the anodic current peak compared to the behavior at Pt. Redox couples having E° in the vicinity of +0.1 exhibit behavior similar to TMPD. Such systems appear to be essentially reversible in the dark at $MoSe_2$ at low scan rates. At fast scan rates such couples depart from reversible behavior in the dark in that the anodic current peak moves more positive and peak current as a function of scan rate departs from the expected (scan rate)$^{1/2}$ dependence for a reversible couple.[11]

The third class of redox couples are those having E° somewhat positive of +0.2. Such couples are not oxidizable in the dark at n-type $MoSe_2$, but upon $\geq E_g$ illumination the oxidation of the reduced form of the couple can be effected at a more negative potential than at Pt. The cyclic voltammetry of this class is represented by [biferrocene]$^{+/0}$, E° = +0.30 (Figure 2).

Thus, the first three classes of redox couples would appear to give electrochemistry expected for an n-type semiconductor having

Scheme I. Interface Energetics for an "Ideal" n-Type Semiconductor/Liquid Interface

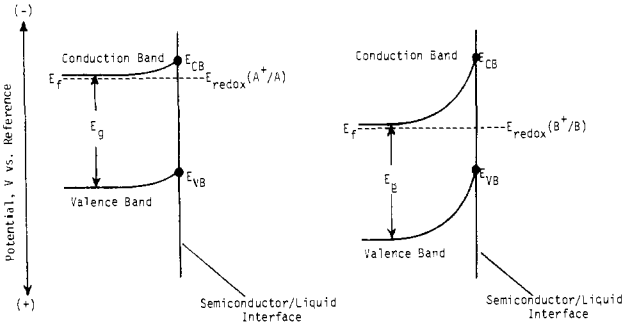

$E_{FB} \approx -0.2$ V vs. SCE.[6,12] Scheme I depicts the interface energetics for an ideal semiconductor/liquid electrolyte junction. Couples more negative than E_{CB} are reversible, and no photoeffects are found, since E° is in the conduction band and the n-type material has electrons as the majority charge carrier.[6,12] Couples having E° somewhat positive of E_{CB} give a photoanodic peak that is more negative than at a reversible electrode such as Pt. No oxidation for class III couples is observable in the dark; oxidation requires the photogeneration of holes, the minority carrier, that would have an oxidizing power no greater than the position of E_{VB}. The extent to which the photoanodic peak is more negative than the anodic peak at Pt is a measure of the output photovoltage from the photoanode. The maximum photovoltage is expected to be given by eq 1.

The fourth class of redox couples, however, do not behave as would be expected from the ideal model for a semiconductor/liquid electrolyte junction. Couples having E° more positive than +0.7 belong to this fourth class of redox couples and are typified by the [*fac*-$BrRe(CO)_3L]^{+/0}$ complex (Figure 3). These couples show

(11) Nicholson, R. S.; Shain, I. *Anal. Chem.* **1964**, *36*, 706.

(12) Frank, S. N.; Bard, A. J. *J. Am. Chem. Soc.* **1975**, *97*, 7427.

Scheme II. Interface Energetics for an n-Type Semiconductor/Liquid Interface When Fermi Level Pinning Applies

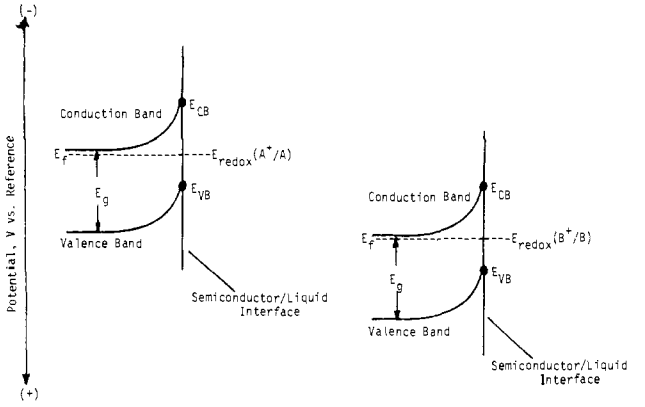

a photoanodic peak that is ~0.4 V more negative than the anodic peak at Pt. Importantly, the 0.4 V output voltage is independent of $E°$ for couples out to +1.5 V. The ideal model would predict a larger output photovoltage as $E°$ becomes positive according to eq 1. Another inconsistency is that photoeffects can be observed for a range of $E°$'s that exceeds E_g of $MoSe_2$. The $[TMPD]^0 \rightarrow [TMPD]^+$ photocurrent onset is at ~−0.2 V vs. SCE that would establish E_{CB} at ~−0.3 V vs. SCE and E_{VB} at +1.1 V vs. SCE, since E_g = 1.4 eV and the donor density of $MoSe_2$ places E_{CB} about 0.1 V more negative than E_{FB}. Thus, the maximum oxidizing power of photogenerated holes should be +1.1 V, and we should be unable to effect the uphill oxidation of the reduced form of a couple having $E°$ more positive than this value. But several reagents such as the *fac*-$BrRe(CO)_3L$ are photooxidizeable at illuminated n-type $MoSe_2$, and the photoanodic peak is ~0.4 V more negative than at Pt and yet $E°$ is more positive than +1.1 V. A third inconsistency with the ideal semiconductor/liquid electrolyte model is that reduction peaks for oxidized species can be significantly more positive than the ~−0.2 V E_{FB} value. Finally, we find that redox reagents such as biferrocene that have two one-electron oxidations with different $E°$'s give two one-electron waves at illuminated n-type $MoSe_2$ rather than one two-electron wave as would be expected within the framework of the ideal model for such interfaces.[6,13]

Oxidation of hexamethylbenzene is irreversible at Pt, but the position of the anodic current peak is ~+1.6 V vs. SCE. We find that hexamethylbenzene can be oxidized at illuminated n-type $MoSe_2$ with a photoanodic current peak at +1.2 V vs. SCE—again about 0.4 V more negative than at Pt. Study of redox couples having $E°$ significantly more positive than +1.6 V vs. SCE (e.g., *fac*-$[(CH_3CN)Re(CO)_3(phen)]^{2+/+}$ (phen = 1,10-phenanthroline), $E°$ = +1.8 V vs. SCE) cannot be studied at illuminated n-type $MoSe_2$ because we find a large photoanodic background current in CH_3CN/0.1 M $[n\text{-}Bu_4N]ClO_4$ onsetting at potentials in the range of +1.2 V vs. SCE. This current is presumably the photoanodic decomposition of the $MoSe_2$ that onsets at ~+0.5 V vs. SCE in aqueous electrolyte solutions. It is this ~0.7 V more positive photoanodic decomposition onset in CH_3CN that allows the competitive oxidation of species such as Cl^-.[5] Perhaps in other solvent/electrolyte combinations the photoanodic decomposition can be shifted even more positive, since the solvation of the photoanodic decomposition products is a key term in the thermodynamics for this process.[14] For now, we note that systems requiring +1.6 V vs. SCE can be oxidized ~0.4 V uphill at illuminated n-type $MoSe_2$ and that couples having $E°$'s in the range +0.7 to +1.6 V vs. SCE appear to give essentially a constant output. Figure 3 includes data for $[TMPD]^{2+/+}$ and *fac*-$[BrRe(CO)_3L]^{+/0}$ in the same solution showing the same negative shift in anodic current peak for these two disparate couples.

Since the reagents belonging to the fourth class of redox couples do not behave according to the ideal model[6] at illuminated n-type $MoSe_2$, we propose that Fermi level pinning[7,10] applies to this set of reagents. Schemes I and II compare the interface situation within the framework of the ideal model and compare it when Fermi level pinning applies. Fermi level pinning refers to a situation where the photovoltage is independent of E_{redox} for a significant variation in E_{redox}. That is, for the variation in E_{redox} there is a constant potential drop across the space-charge region of the semiconductor and a variation in the drop across the Helmholtz layer. Such a model[7,10] accommodates the finding that (i) photoeffects are found for redox couples having $E°$'s spanning a range greater than E_g, (ii) reduction can be found at potentials more positive than $E_{FB} \approx -0.2$ V vs. SCE, and (iii) multielectron redox couples can give multi one-electron waves at illuminated n-type $MoSe_2$ with a potential spacing near that found at Pt, though each one-electron wave is shifted to a more negative potential than at Pt. The evidence for photoelectrochemical effects for redox couples whose $E°$'s span a greater range than the separation of E_{CB} and E_{VB} of $MoSe_2$ is strengthened by noting that $MoSe_2$ exhibits optical properties consistent with an indirect band gap at ~1.1 eV.[15] This means that the E_{VB} position would be at +0.8 V vs. SCE not at +1.1 V vs. SCE as would be assigned for a 1.4-eV band gap material.

Fermi level pinning can be attributed to a significant density of surface states situated between E_{CB} and E_{VB}[7] or to carrier inversion[10] such that the n-type material develops a near surface "p-type" region due to the fact that the Fermi level in this region becomes closer to the top of the valence band. The surface states between E_{CB} and E_{VB} seem to provide a better rationale for reductions that occur more positive than E_{FB}.[12,13] But the carrier inversion model provides a better rationale for the fact that some redox couples behave more or less as expected (E_{redox} more negative than +0.7 V vs. SCE) while others give constant output photovoltage independent of E_{redox}. The layered MY_2 semiconductors are judged to be relatively free of intrinsic surface states,[16] but this does not rule out an important role for "extrinsic" surface states from oxide or other impurity material on the surface during operation. Whatever the origin of the Fermi level pinning, it appears that the $MoSe_2$ photoanodes can be used to effect oxidations that would be regarded as impossible within the ideal model[6] where E_{CB} and E_{VB} remain fixed.

Other small band gap, n-type semiconductors appear to exhibit Fermi level pinning. For example, n-type CdTe[17] (E_g = 1.4 eV) and GaAs (E_g = 1.4 eV)[7] both give a photovoltage that is independent of E_{redox} for a range spanning more than the separation of E_{VB} and E_{CB}. Unlike $MoSe_2$, these materials give photovoltages for very negative redox couples where the semiconductor could have an accumulation layer (rather than carrier inversion layer). In these cases it would appear that the surface state model more adequately accounts for the large range of redox couples that give a constant photovoltage.

Aside from surface states and carrier inversion, it is worth noting that hot carrier injection is another possible rationale for photovoltages from redox couples situated more positive than E_{VB} of n-type semiconductors.[18] Unusually strict criteria need apply for this rationale to apply, and it does not appear likely that hot carrier injection will apply to $MoSe_2$/liquid interfaces.

Semiconductor/metal (Schottky barrier) interfaces also exhibit Fermi level pinning.[19] In analogy to the semiconductor/liquid junctions, it is sometimes difficult to determine what causes the

(13) Bocarsly, A. B.; Walton, E. G.; Bradley, M. G.; Wrighton, M. S. *J. Electroanal. Chem.* **1979**, *100*, 283.
(14) Bard, A. J.; Wrighton, M. S. *J. Electrochem. Soc.* **1977**, *124*, 1706.
(15) (a) Wilson, J. A.; Yoffe, A. D. *Adv. Phys.* **1979**, *18*, 193. (b) Goldberg, A. M.; Beal, A. R.; Levy, F. A.; Davis, E. A. *Philos. Mag.* **1975**, *32*, 367; (c) Kautek, W.; Gerischer, H.; Tributsch, H. *J. Electrochem. Soc.*, in press and private communication.
(16) (a) Kama, A.; Enari, R. *Conf. Ser.-Inst. Phys.* **1979**, *No. 43*, Chapter 5. (b) McMenamin, J. C.; Spicer, W. E. *Phys. Rev. B* **1977**, *16*, 5474.
(17) Aruchamy, A.; Wrighton, M. S. *J. Phys. Chem.*, in press.
(18) (a) Nozik, A. J.; Bourdreaux, D. S.; Chance, R. R.; Williams, F. *Adv. Chem. Ser.* **1980**, *No. 184*, 155. (b) Boudreaux, D. S.; Williams, F.; Nozik, A. J. *J. Appl. Phys.* **1980**, *51*, 2158.
(19) (a) Mead, C. A.; Spitzer, W. G. *Phys. Rev. A* **1964**, *134*, 714. (b) McGill, T. C. *J. Vac. Sci. Technol.* **1974**, *11*, 935.

Scheme III. Classification of Redox Couples Examined at $MoSe_2$ Photoanodes

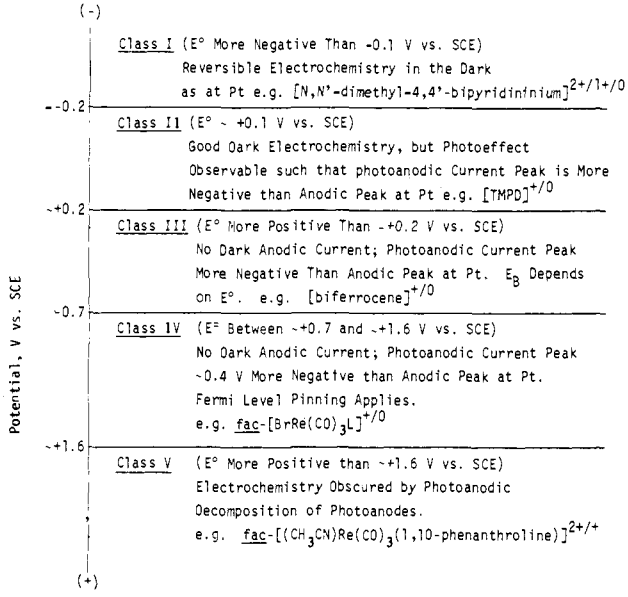

output photovoltage to be independent of the contacting metal. Direct experimental probes of the interface in situ will be necessary to determine the origin of this phenomenon.

Fermi level pinning has been invoked for several other small band gap semiconductors immersed in liquid electrolytes.[7-9,17] For p-type Si it would appear that couples having $E°$ more negative than 0.0 V vs. SCE will exhibit a constant photovoltage.[9] Thus, for this elemental, p-type semiconductor a redox couple having $E°$ more negative than 0.0 V vs. SCE would give the same photovoltage and could prove useful in a stable device. It is crucial that p-type Si is chemically durable at very negative potentials. All n-type materials seem to undergo photoanodic decomposition at some positive potential,[14] and though Fermi level pinning may apply, chemical reality precludes the use of very positive couples. For n-type $MoSe_2$, couples more positive than +1.6 V vs. SCE in CH_3CN appear to be useless, since n-type $MoSe_2$ undergoes photoanodic decomposition in this range. However, the MY_2 materials seem to be durable at significantly more positive potentials than any other nonoxide materials studied to date. For example, n-type CdTe[17] and n-type GaAs[20] materials having a direct 1.4 eV value of E_g undergo photoanodic decomposition at 0.0 V vs. SCE in CH_3CN solutions in contrast to the +1.2 V vs. SCE associated with the direct gap, E_g = 1.4 eV, n-type $MoSe_2$. Thus, we note a fifth class of redox couples: those where $E°$ is significantly more positive than potentials that give photoanodic decomposition. Scheme III summarizes the findings for redox couples studied at $MoSe_2$ photoanodes. We propose to use this classification in discussing redox behavior at n-type semiconductor/liquid junctions. A similar classification of redox systems would be possible for p-type electrodes except that class I would be associated with positive couples overlapping the valence band and the photogenerated minority carrier is the electron. This classification scheme will be elaborated in a subsequent report concerning p-type InP.[21]

In our earlier study[4] of n-type MoS_2 we found many redox couples that give photoanodic current onsets at ~+0.3 V vs. SCE, but the most positive redox couple examined has an $E°$ of ~+1.25 V vs. SCE. The direct gap of MoS_2 is 1.7 eV, but the indirect gap is at ~1.2 eV from optical measurements.[15] This means that the E_{VB} is in fact at ~+1.4 V vs. SCE not the ~1.9 V vs. SCE assignment based on the E_g = 1.7 eV, direct.[4] We have now examined the cyclic voltammetry of $[(CH_3CN)Re(CO)_3(2,2'\text{-biquinoline})]^{2+/+}$, $E°$ = +1.8 V vs. SCE, at illuminated MoS_2. We find that the photoanodic peak for the oxidation of the reduced form of the couple is ~450 mV more negative than the corresponding peak at Pt. Since the $E°$ for this couple is +1.8 V vs. SCE, the photoeffects for this system suggest that Fermi level pinning also applies to MoS_2 contacted by fairly positive redox couples. The $[BrRe(CO)_3L]^{+/0}$, $E°$ = 1.45 V vs. SCE (see Table I), was also examined at illuminated n-type MoS_2 in CH_3CN, and the photoanodic peak is also ~450 mV more negative than at Pt. Our previous data for $Ru(bpy)_3^{3+/2+}$ (bpy = 2,2'-bypyridene), $E°$ = 1.25 V vs. SCE, showed a 470-mV negative shift, while $[1,1'\text{-diacetylferrocene}]^{+/0}$, $E°$ = 0.83 V vs. SCE, only showed a ~280-mV negative shift. All of the couples for which photoanodic peaks are observed show a dark reduction current at a potential positive of the "E_{FB}" at +0.3 V. This fact implicates surface states as we previously noted,[4] but now we additionally conclude that couples for which $E°$ is more positive than +1.0 V can belong to class IV. The output photovoltage for the class IV couples is ~450 mV. Photoanodic decomposition for MoS_2 in $CH_3CN/[n\text{-}Bu_4N]ClO_4$ onsets at ~+1.4 V vs. SCE and couples ~0.4 V more positive than this are thus assigned to class V.

b. Conversion of Light to Electricity Employing Halogen/Halide Redox Couples. We discovered that n-type $MoSe_2$ and MoS_2 are stable photoanodes in CH_3CN electrolyte solutions containing halogen/halide, X_n^-/X^- (X = Cl, Br, I) redox couples.[4,5] By way of contrast, only the X = I couple is believed to yield a stable photoelectrochemical cell when H_2O is the solvent. As indicated above, the onset of photoanodic decomposition of the photoanodes in H_2O is at ~+0.5 V vs. SCE which is more negative than the $E°$ of the Br_2/Br^-, $E°$ = +0.63 V vs. SCE, and the Cl_2/Cl^-, $E°$ = +1.1 V vs. SCE. In CH_3CN these more positive $E°$'s are more negative than the onset potential for photoanodic decomposition. Thus, the use of CH_3CN solvent allows the study of both Br^- and Cl^- oxidations at the illuminated photoanodes. We have made a comparison of the efficiency of n-type $MoSe_2$- and MoS_2-based photoelectrochemical cells where eq 2 and 3 represent the photoanode and cathode reactions, respectively. Additionally, we have compared the results in CH_3CN for X = I with those in H_2O for X = I that does give a stable cell.

$$nX^- \rightarrow X_n^- + (n-1)e^- \text{ (photoanode)} \quad (2)$$

$$X_n^- + (n-1)e^- \rightarrow nX^- \text{ (cathode)} \quad (3)$$

$$X = Cl, Br, I$$

At first it would seem appropriate to compare the X_n^-/X^- systems with the couples for which data are given in Table I. However, all of the systems in Table I are outer-sphere, one-electron redox reagents, unlike the halogen couples that involve at least two-electron processes. Nonetheless, we have carried out cyclic voltammetry of X^- at illuminated $MoSe_2$. Generally, we do find that anodic current peaks at Pt are shifted to a more negative potential at illuminated $MoSe_2$ photoanodes. None of the X^- species at ~1 mM are oxidizable in the dark at n-type $MoSe_2$ at 100-mV/s scan rates. Thus, we place the X = I and Br couples in the class III category, and the Cl_2/Cl^- system is put in class IV on the basis of the fact that $E°$ = +1.1 V vs. SCE is in the ~+0.7 to +1.6 V vs. SCE range. At the low concentrations (~1 mM) of X^- used in cyclic voltammetry we find that the extent of the negative shift is ~0.1 V for Br^- and I^- and ~0.3 V for Cl^-. These data are not as reproducible as for the couples in Table I nor are the current waves as clean as for the couples in Table I. Even at Pt-wire electrodes the cyclic voltammetry is not as clean and reproducible as would be desirable presumably due to adsorption onto Pt and corrosion of the Pt. But the general photoeffects expected for class III (X = I, Br) and class IV (X = Cl) redox couples are found.

Comparison of steady-state photocurrent–voltage curves in CH_3CN containing ~1.0 M X^- reveals that all three halides behave in a similar manner except that the onset of photocurrent is ordered such that I^- oxidation is most negative (onset ~0.1 V

(20) Dominey, R. N.; Wrighton, M. S., to be submitted for publication (results for GaAs).
(21) Dominey, R. N.; Lewis, N. S.; Wrighton, M. S, to be submitted for publication.

Table II. Data from Steady-State Photocurrent-Voltage Curves for X^- Oxidation at Illuminated $MoSe_2$[a]

X^- (concn, M)	E° (X_n^-/X^-), V vs. SCE	input power,[b] mW	photocurrent onset, V vs. SCE	Φ_e at +1.0 V vs. SCE[c]
Cl^- (1.0)	+1.1	0.16	~+0.44	0.60
		0.60	~+0.36	0.62
		3.3	~+0.32	0.62
Br^- (1.0)	+0.7	0.17	~+0.26	0.55
		0.61	~+0.20	0.57
		3.2	~+0.15	0.52
I^- (0.9)	+0.3	0.16	~+0.05	0.52
		0.60	~+0.05	0.52
		3.2	~−0.10	0.56

[a] All data are for stirred CH_3CN solutions containing 1.0 M $[Et_4N]Cl$, 1.0 M $[Et_4N]Br$, or 0.9 M $[n\text{-}Bu_4N]I$ at 25 °C under Ar. [b] Input illumination from a He-Ne laser, 632.8 nm, having a 0.6-mm beam diameter. [c] Quantum yield for electron flow corresponding to X^- oxidation at +1.0 V vs. SCE.

vs. SCE) and Cl^- oxidation is most positive (onset ~+0.3 V vs. SCE), leaving Br^- oxidation in between (onset ~+0.15 V vs. SCE). These data and other features are summarized in Table II. As shown, the quantum yield at a positive potential is high in all cases and independent of light intensity over the range studied. The electrode surfaces are good specular reflectors, accounting for a significant loss in current. The rectangularity of the photocurrent–voltage curves is very good for all systems at the lowest intensity but declines significantly at the highest intensity. The shape of curves is independent of X^-; all show a region where photocurrent is insensitive to voltage (hole limited current) that begins ~0.4 V positive of the onset voltage of the lowest intensities.

The difference of importance, with respect to optical energy conversion efficiency, is the onset of photocurrent for X^- oxidation relative to the E° of the X_n^-/X^- couple. This is an indication that the output voltage from n-type $MoSe_2$-based cells employing the X_n^-/X^- couples will have an output voltage that depends on X with the order Cl > Br > I. Indeed, for the solutions used to determine data given in Table II, we find that oxidation of X^- at Pt has about the same onset for X = I and is ~0.3 V more positive for X = Br and ~0.5 V more positive for X = Cl. Thus, solutions containing significant quantities of X_n^- in addition to X^- yield a light to electricity conversion efficiency that depends on X in the order Cl > Br > I (Table III and Figure 4). The main reason for the efficiency variation is output photovoltage variation, since the shape of the steady-state current potential curves and the limiting quantum yield for electron flow are independent of X.

The rather poor efficiency associated with the I_3^-/I^- redox couple in CH_3CN stands in contrast to the rather good efficiency associated with this couple when H_2O is the solvent. With the same electrodes that give poor properties in CH_3CN we find rather good properties in H_2O solvent. Conversion efficiencies of the order of 3% can be realized in H_2O solvent containing the I_3^-/I^- couple. We believe the improved efficiency to result from two factors that both lead to improved output voltage. First, the formal potential of the I_3^-/I^- couple is somewhat more positive in H_2O than in CH_3CN, and, second, there appears to be a somewhat more negative onset of photoanodic current and the rectangularity is improved in H_2O compared to CH_3CN. The latter effects are likely due to a rather strong interaction of I^- with the $MoSe_2$ surface in H_2O. Adsorption of anions onto the photoanode is known to effect a negative shift of E_{FB}. Adsorption of I^- in CH_3CN solution likely occurs as well, but the effects are less pronounced.

In the case of MoS_2, the effect of I^- adsorption in H_2O also results in significantly improved efficiency compared to that of CH_3CN (Table IV). But even in CH_3CN the adsorption effect of I^- is pronounced. For example, $E^\circ(I_3^-/I^-)$ = +0.2 V vs. SCE in CH_3CN would indicate for n-type MoS_2 that class II behavior would be expected, as we found for $[ferrocene]^{+/0}$ having E° = +0.38 V vs. SCE. But we actually find that I^- exhibits class III behavior at n-type MoS_2; i.e., we find no oxidation in the dark at ~1 mM concentration and 100-mV/s scan rate and photooxidation can be effected at a potential more negative than at Pt. As for $MoSe_2$, the efficiency for n-type MoS_2-based cells is a little larger when $CH_3CN/Cl_2/Cl^-$ is used than when the $H_2O/I_3^-/I^-$ system is used. Further, the MoS_2 appears to be unstable as a photoanode in aqueous solutions of ~1.0 M Br or Cl^- but is durable as a photoanode in CH_3CN solutions of these halides. The efficiency for MoS_2-based cells employing CH_3CN solutions of X_n^-/X^- is ordered according to X = Cl > Br > I, as we find in $MoSe_2$ (Table IV and Figure 5). Comparing $MoSe_2$ and MoS_2, we find that at 632.8 nm the $MoSe_2$ is somewhat more efficient

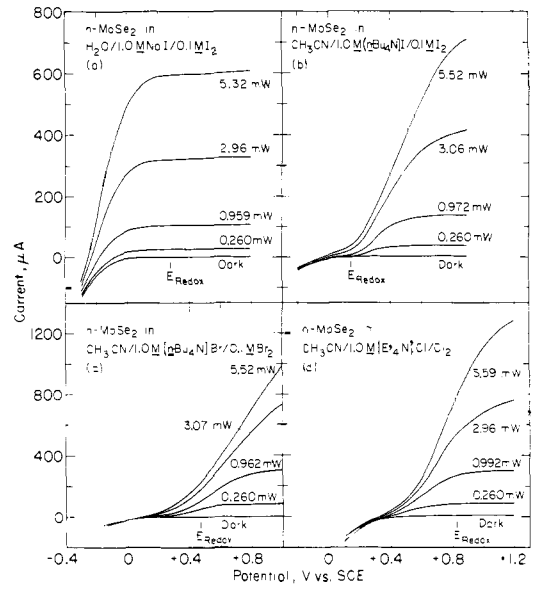

Figure 4. Steady-state photocurrent–voltage curves for $MoSe_2$ (photoanode) based cells in various electrolyte solutions as a function of input optical power (632.8 nm). For power or current density multiply values given by 354 cm^{-2}. E_{redox} denotes the solution potential in each case. These data are for $MoSe_2$ sample no. 3 in Table III.

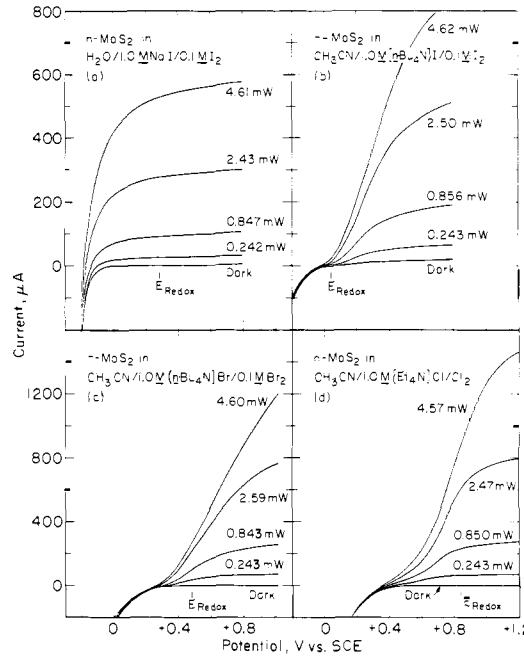

Figure 5. Steady-state photocurrent–voltage curves for MoS_2 (photoanode) based cells in various electrolyte solutions as a function of input optical power (632.8 nm). For power or current density multiply values given by 31.8 cm^{-2}. E_{redox} denotes the solution potential in each case. These data are for MoS_2 sample No. 1 in Table IV.

Table III. Conversion Efficiency for n-Type $MoSe_2$-Based Cells Employing X_n^-/X^- Couples[a]

$MoSe_2$ sample	solvent/X_n^-/X^- (E_{redox}, V vs. SCE)	input pwr,[b] mW	Φ_e at E_{redox}[c]	max E_V, mV (E_V at η_{max}, mV)[d]	η_{max},[e] %	fill factor[f]
1	$CH_3CN/Cl_2/Cl^-$ (+1.05)	0.26	0.73	360 (250)	5.9	0.46
		1.0	0.65	410 (250)	5.4	0.41
		2.4	0.58	450 (250)	5.3	0.40
		3.3	0.55	450 (250)	4.4	0.34
		5.9	0.45	480 (250)	3.3	0.30
2	$CH_3CN/Cl_2/Cl^-$ (+0.96)	0.26	0.65	460 (350)	7.5	0.50
		0.94	0.68	500 (300)	7.2	0.40
		2.6	0.66	540 (250)	4.0	0.22
		4.6	0.48	550 (250)	2.6	0.19
3	$CH_3CN/Cl_2/Cl^-$ (+1.00)	0.27	0.50	370 (250)	4.8	0.51
		1.0	0.56	440 (250)	5.2	0.42
		3.1	0.41	470 (230)	3.2	0.33
		5.6	0.43	490 (230)	2.7	0.25
3	$CH_3CN/Cl_2/Cl^-$ (+0.83)	0.26	0.60	440 (250)	5.2	0.38
		0.99	0.52	460 (220)	3.1	0.25
		3.0	0.34	490 (180)	1.6	0.19
		5.6	0.28	500 (170)	1.2	0.16
4	$CH_3CN/Br_2/Br^-$ (+0.53)	0.30	0.29	340 (150)	1.4	0.29
		0.77	0.31	390 (150)	1.1	0.18
		2.0	0.18	420 (150)	0.6	0.15
		3.5	0.11	430 (150)	0.4	0.15
5	$CH_3CN/Br_2/Br^-$ (+0.53)	0.30	0.23	290 (150)	0.8	0.24
		0.77	0.23	330 (150)	0.7	0.18
		2.0	0.14	370 (150)	0.4	0.15
3	$CH_3CN/Br_2/Br^-$ (+0.47)	0.26	0.38	280 (150)	1.1	0.20
		0.96	0.21	300 (130)	0.5	0.17
		3.1	0.11	350 (130)	0.3	0.17
		5.5	0.08	370 (150)	0.3	0.17
6	$CH_3CN/I_3^-/I^-$ (+0.085)	0.22	0.04	90 (40)	0.05	0.28
		0.75	0.03	100 (40)	0.04	0.30
		2.2	0.03	130 (40)	0.03	0.19
		4.6	0.03	160 (40)	0.03	0.17
7	$CH_3CN/I_3^-/I^-$ (−0.02)	0.26	0.14	60 (30)	0.09	0.22
		1.0	0.11	100 (60)	0.14	0.25
		3.3	0.08	150 (60)	0.12	0.20
		6.4	0.05	170 (60)	0.08	0.19
3	$CH_3CN/I_3^-/I^-$ (+0.05)	0.26	0.02	20 (5)	0.04	0.37
		0.97	0.02	90 (50)	0.02	0.25
		3.1	0.02	160 (90)	0.03	0.23
		5.5	0.01	190 (90)	0.02	0.21
3	$H_2O/I_3^-/I^-$ (+0.28)	0.26	0.20	360 (270)	2.0	0.55
		0.96	0.21	460 (300)	2.9	0.58
		3.0	0.21	510 (330)	2.7	0.49
		5.3	0.22	540 (330)	2.7	0.45
7	$H_2O/I_3^-/I^-$ (+0.28)	0.26	0.36	360 (250)	3.4	0.51
		1.1	0.38	450 (250)	3.9	0.45
		3.6	0.32	480 (250)	2.7	0.34
		6.6	0.27	500 (250)	2.0	0.29

[a] All data are for stirred solutions of 1.0 M $[Et_4N]Cl$, 1.0 M $[n\text{-}Bu_4N]Br$, 1.0 M $[n\text{-}Bu_4N]I$, NaI, or LiI with appropriate amounts of X_2 added to bring E_{redox} of the solution to the indicated value. Solutions are kept under Ar. [b] Input optical power from a 632.8 nm (0.6-mm beam diameter) He-Ne laser. For power density multiply by 354 cm^{-2}. [c] Quantum yield for electron flow at an n-type $MoSe_2$ potential equal to E_{redox} of the solution. This corresponds to the short circuit quantum yield. [d] Open circuit photovoltage and output at the maximum power point is given in parentheses. [e] Maximum efficiency for conversion of 632.8-nm light to electricity. [f] Fill factor is a measure of the rectangularity of the output photovoltage-photocurrent curve and is defined to be (max power out)/(max E_V × short-circuit photocurrent).

under the same conditions in CH_3CN. Likewise in $H_2O/I_3^-/I^-$ the $MoSe_2$-based cell is somewhat more efficient.

We previously communicated[5] results, indicating a large improvement in efficiency for the $CH_3CN/Cl_2/Cl^-$ solvent/redox system by using $MoSe_2$ photoanodes rather than MoS_2 photoanodes.[4] Data in Tables III and IV and Figures 4 and 5 show that our $MoSe_2$ samples do indeed give a higher efficiency at an order of magnitude greater input optical power density. However, the improvement in 632.8-nm conversion efficiency is not quite as great as originally estimated[5] perhaps owing to the use of a relatively poor MoS_2 sample coupled with a relatively low concentration (0.2 M) of Cl^- for the MoS_2-based cell. An advantage for $MoSe_2$-based cells can still be realized from the smaller value of the direct band gap for $MoSe_2$ (1.4 eV) compared to that for MoS_2 (1.7 eV).

The efficiencies given in Tables III and IV for the $H_2O/I_3^-/I^-$ system are of the same order as previously reported by other groups[1,2] but are not as high as the best. Such variations are expected among different samples depending on their surface or bulk properties. Our data indicate that the best efficiencies will be found for cells employing the $CH_3CN/Cl_2/Cl^-$ system.

Experimental Section

Materials. Single crystals of $MoSe_2$ (ρ_{RT} = 6.2 Ω cm) were grown by vapor phase transport by using Br_2 or I_2 as the transport agent. The thin, flat crystals were of 0.01–0.2 cm^2 in exposed area (001 face). All samples were found to be n-type from photoeffects observed. N-type MoS_2 samples were from the same source previously used.[4] Spectrograde CH_3CN, ferrocene, I_2, Br_2, Cl_2, acetylferrocene, hexamethylbenzene, LiCl, $[Et_4N]Cl$, $[n\text{-}Bu_4N]Br$, LiI, NaI, and $[n\text{-}Bu_4N]I$ were used as obtained from commercial sources after the absence of electroactive impurities was ensured by examining electrochemistry at a Pt electrode. 1,1′-Diacetylferrocene was purified by column chromatography, and *N,N′,N′,N′*-tetramethyl-*p*-phenylenediamine (TMPD) was purified by sublimation. Biferrocene (BF) and decamethylferrocene were prepared as de-

Table IV. Output of MoS_2-Based Photoelectrochemical Cells Employing X_n^-/X^- Redox Couples

MoS_2 sample	solvent/X_n^-/X^- (E_{redox}, V vs. SCE)	input power, mW	Φ_e at E_{redox}	max E_V, mV (V at η_{max}, mV)	η_{max}, %	fill factor
1	CH_3CN/1.0 M $[Et_4N]Cl/Cl_2$ (+0.84)	0.243	0.52	420 (240)	3.75	0.33
		0.850	0.53	440 (160)	2.6	0.22
		2.47	0.48	460 (150)	1.8	0.16
		4.57	0.38	480 (150)	1.4	0.15
2	CH_3CN/1.0 M $[Et_4N]Cl/Cl_2$ (+0.84)	0.243	0.48	300 (120)	2.0	0.27
		0.847	0.53	340 (120)	2.0	0.22
		2.44	0.45	370 (120)	1.4	0.17
		4.57	0.35	290 (120)	1.1	0.15
1	CH_3CN/1.0 M $[n\text{-}Bu_4N]Br$/0.1 M Br_2 (+0.48)	0.240	0.33	170 (80)	0.67	0.24
		0.843	0.26	200 (80)	0.52	0.20
		2.56	0.19	230 (80)	0.41	0.19
		4.60	0.13	240 (80)	0.30	0.18
2	CH_3CN/1.0 M $[n\text{-}Bu_4N]Br$/0.1 M Br_2 (+0.49)	0.240	0.23	70 (20)	0.08	0.14
		0.847	0.11	110 (40)	0.10	0.17
		2.44	0.08	140 (60)	0.09	0.17
		4.56	0.06	170 (60)	0.09	0.16
1	CH_3CN/1.0 M $[n\text{-}Bu_4N]I$/0.1 M I_2 (+0.04)	0.243	no measurable output			
		0.856	<0.01	30 (10)	0.002	0.22
		2.50	0.01	50 (20)	0.004	0.18
		4.60	0.01	55 (20)	0.005	0.21
2	CH_3CN/1.0 M $[n\text{-}Bu_4N]I$/0.1 M I_2 (+0.12)	0.242				
		0.847	no measurable output			
		2.48				
		4.58				
1	H_2O/1.0 M NaI/0.1 M I_2 (+0.28)	0.242	0.20	380 (280)	2.1	0.53
		0.847	0.21	410 (280)	2.3	0.53
		2.43	0.22	450 (330)	2.6	0.51
		4.61	0.22	470 (330)	2.6	0.49
2	H_2O/1.0 M NaI/0.1 M I_2 (+0.28)	0.250	0.16	340 (230)	1.5	0.52
		0.859	0.21	410 (310)	2.3	0.52
		2.46	0.20	440 (330)	2.3	0.51
		4.66	0.21	460 (330)	2.6	0.51

[a] All data are for 632.8-nm excitation of n-type MoS_2 (photoanode) in cells employing the indicated solvent/X_n^-/X^- systems. For input power density multiply indicated values by 31.8 cm^{-2}. Other table headings same as in Table III for the $MoSe_2$-based cells.

scribed in the literature.[22,23] *fac*-$BrRe(CO)_3L$, *fac*-$[(CH_3CN)Re(CO)_3(phen)]^+$, *fac*-$[(CH_3CN)Re(CO)_3(2,2'\text{-biquinoline})]^+$, and *N,N'*-dimethyl-4,4'-bipyridinium were samples previously synthesized in this laboratory.[24] $[n\text{-}Bu_4N]ClO_4$, from Southwestern Analytical Chemicals, was vacuum dried at 70 °C for 24 h.

Electrode Preparation. $MoSe_2$ electrodes (~0.01–0.2 cm^2 exposed area) were fabricated as follows. Satisfactory electrical contacts were made by rubbing Ga–In eutectic on one side of a crystal and mounting (with conducting silver epoxy) onto a coiled copper wire. The copper wire lead was passed through 4-mm Pyrex tubing and the assembly insulated with ordinary epoxy, leaving only the $MoSe_2$ 001 face exposed to the electrolyte. MoS_2 electrodes were prepared from materials previously described.[4]

Electrochemical Equipment and General Procedures. Cyclic voltammograms were recorded in CH_3CN/0.1 M $[n\text{-}Bu_4N]ClO_4$ solutions with redox reagent concentration at ~1 mM in every case and current–voltage data in solutions as indicated by using a PAR Model 173 potentiostat equipped with a PAR Model 175 programmer. Scans were recorded with a Houston Instruments Model 2000 X-Y recorder. Except where otherwise stated, a single compartment cell was used employing a standard three-electrode configuration with a Pt counterelectrode and a saturated calomel reference electrode (SCE). All measurements are for 25 °C.

For all experiments the light source was a He–Ne laser (Coherent Radiation) that provided 632.8-nm light of up to ~2 W/cm^2. The power was adjusted by using neutral density glass filters or, for cyclic voltammetry, by expanding the beam to provide ~50 mW/cm^2. The intensity of the irradiation was determined by using a Tektronix J16 digital radiometer equipped with a J6502 probe.

Electrodes were routinely checked prior to use and rechecked at the conclusion of most experiments by scanning in a 0.5 mM ferrocene/0.1 M $[n\text{-}Bu_4N]ClO_4/CH_3CN$ electrolyte at 100 mV/s ($MoSe_2$). Under illumination, good electrodes show a photocurrent onset for the oxidation of ferrocene to ferricenium at ~0 V vs. SCE with a well-defined photoanodic peak at ~+0.2 V vs. SCE. MoS_2 photoanodes were checked as previously described[4] by using [TMPD] as the redox active material.

Note Added in Proof: We have recently found that both n-type MoS_2 and $MoSe_2$ are stable photoanodes for Cl_2 generation from aqueous 15 M LiCl solutions: Kubiak, C. P.; Schneemeyer, L. F., Wrighton, M. S. *J. Am. Chem. Soc.*, in press.

Acknowledgment. We thank the Office of Naval Research for partial support of this research. Support from the M.I.T. Cabot Solar Energy Fund and GTE Laboratories is also gratefully acknowledged. M.S.W. has been the recipient of a Dreyfus Teacher-Scholar Grant, 1975–1980. Samples of characterized $MoSe_2$ were kindly supplied by A. Stacy and Professor M. J. Sienko of Cornell University. Valuable discussions with Professors H. Gerischer and A. J. Bard and Dr. A. J. Nozik are acknowledged.

(22) Rudie, A. Ph.D. Thesis, M.I.T., 1978.
(23) King, R. B.; Bisnette, M. B. *J. Organomet. Chem.* **1967**, *8*, 287.
(24) (a) Fredericks, S. M.; Luong, J. C.; Wrighton, M. S. *J. Am. Chem. Soc.* **1979**, *101*, 7415. (b) Luong, J. C.; Nadjo, L.; Wrighton, M. S. *Ibid.* **1978**, *100*, 5790. (c) Staal, L. H.; Oskam, A.; Vrieze, K. *J. Organomet. Chem.* **1979**, *170*, 235. (d) Luong, J. C., unpublished results.